

# Control and Analysis of a Multimodal Twisted-Winch String Actuator with Embodied Sensing

**Abstract**—We present a novel actuator that combines a twisted string actuator (TSA) with a winch mechanism. This hybrid actuator overcomes TSA limitations such as overtwisting and limited stroke length while still offering the ability for high force output. By integrating the winch, greater stroke and variable transmission ratios are achieved without risking overtwisting. The developed kinematic model forms the backbone of a conventional feedback gain controller with a gain scheduling scheme. We allocate control effort proportionally, guided by the relationship between actuator modes and the resulting string statics and velocity. Using a conductive string, displacement can be measured as a function of the change of electrical resistance, enabling precise control with real-time feedback without wires and encoders compromising the compliance of soft robots. Experiments validate our model and control strategies, showing improved performance and responsiveness. By eliminating the need for rigid end-effector encoders and bulky transmissions, this actuator enhances capabilities for soft robotics and automation while advancing TSA technology.

## I. INTRODUCTION

Twisted string actuators (TSAs) provide mechanical advantage without the need for large transmission systems by transforming rotational motion into linear movement via the twisting of strong strings. Their simplicity and light weight make them ideal for applications where space is limited and low joint inertia is desirable, such as haptic gloves [1], robotic grippers [2], exoskeletons [3], and soft robotic manipulators [4]. TSAs operate by contracting under torsion after exiting a brief torsional elongation phase, a phase that has been observed in some of the earliest work on twisting metal wires and rubber cords done by the physicist Poynting in the 1900s [5], [6].

Despite their advantages, TSAs face challenges such as nonlinear behavior that complicates precise control and the risk of unstable overtwisting, which limits stroke length. Excessive twisting can cause mechanical instability and reduce lifespan [7]. Various solutions have been explored to adjust the transmission ratio and overcome these limitations, including clutches [8], manually adjustable modules [9], passive elastomeric mechanisms [10], and active control of individual string twists [11]. Optimization techniques aim to maximize stroke relative to string length [12]. However, these approaches often fail to fully address limited stroke length, overtwisting issues, and the proportional relationship between force transmission and twisting.

TSAs excel in force output relative to torque input, while winches achieve larger contractions and speeds [13]. To leverage both strengths, an actuator was designed to combine a TSA with a winch mechanism [14]. This integrated twist-winches system offered dynamic adjustment capabilities,

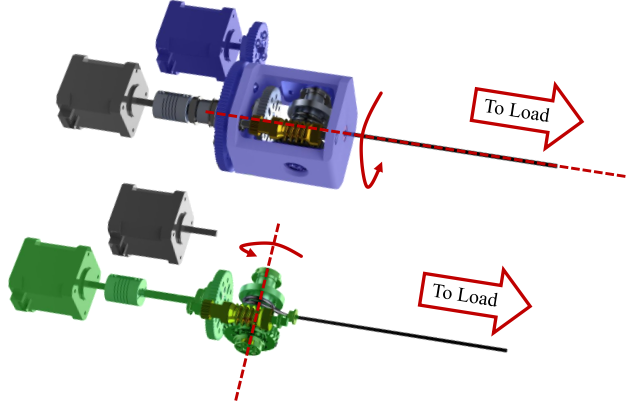


Fig. 1. The TSA/winch hybrid actuator. On top, the turret rotation gear transmission mechanism (shaded in blue) twists the string. Underneath, the winch gear transmission (shaded green) inside the turret winds up the string. Both transmissions are driven by stepper motors.

improving stroke and transmission ratio variability without overtwisting. This study expanded existing models [15], [16] to include the kinetostatics of the winch action and verified them using a rotating turret design that housed a winch on a bevel gear assembly driven by a through-hole shaft [14]. However, precise control typically relies on feedback rather than open-loop models. While an encoder at the string end could provide feedback, using a conductive string maintains the benefits of low inertia, low rigidity, fewer wires, and compactness inherent in soft tendon-driven systems [17]. This approach often requires the use of the conductive strings that are commercially available but are typically more compliant.

Using compliant strings in TSAs presents challenges. More compliant strings produce less strain when twisted, pushing TSAs to overtighten and coil to enhance strain [18]. Although the hybrid winch-TSA mitigates this issue, reduced strain still implies decreased force with increased compliance. At extreme compliance levels, string length can even increase under load when twisted [5], [6], [19]. Compliant strings also suffer from increased hysteresis, reduced lifespan, and creep over time, emphasizing the need for feedback in precise control [20]. Additionally, with lower stiffness materials at high speeds, the system cannot be assumed rigid as in some previous work [21]. Modeling load dynamics and string elasticity has been extensively researched to try to capture this string behavior for TSAs [22]. Overall, the challenges introduced by using a compliant conductive string highlights the necessity of using feedback for precise control.

instead of depending on open-loop models.

Building on previous TSA kinematics models [15], [16] to incorporate the added winching action, we introduce a control strategy that allocates standard feedback controller effort between two stepper motors based on a user-defined factor, which varies between pure twisting and pure winching modes. In doing so, the controller gain is dictated by a carefully tuned gain scheduling method to achieve the desired system responsiveness. This control strategy is developed and experimentally validated by leveraging real-time strain measurements via a conductive string. Measuring string displacement is done directly through electrical resistance similar to past work [20] but in the context of this new hybrid actuator, where different modes may yield different relationships between voltage change and position. This approach allows accurate estimation of contracted length and is effective in improving performance by integrating real-time measurements into the control system to compensate for friction and nonlinear dynamics.

This work begins by first describing the background modeling and proposed control methodologies. We then present simulation and performance data, followed by a discussion of the results. The conclusion summarizes the findings and their implications for soft robotics and automation. Our main contributions are the following:

- 1) A novel actuator that combines both twisting and winch-driven actuation modalities for soft robotic applications.
- 2) A mechanism for providing feedback control through the use of a conductive cable without the need for bulky transmissions and encoders at the end effector.
- 3) Experimental results that validate the performance and capabilities of this mechanism.

The combination of a twist-winch mechanism with conductive string sensing represents a significant step forward in actuator design, offering improved capabilities for a wide breadth of robotic applications.

## II. MODELS AND EQUATIONS

### A. State and Output Variables

The state vector for this twisting-winching string actuator is

$$\mathbf{x} = [X \quad \dot{X} \quad \theta_{\text{eff}} \quad \dot{\theta}_{\text{eff}} \quad \phi_{\text{eff}} \quad \dot{\phi}_{\text{eff}}]^T, \quad (1)$$

where  $X$  is the displacement of the string,  $\theta_{\text{eff}}$  is the effective twisting angle of the string,  $\phi_{\text{eff}}$  is the effective winch angle, and  $\dot{X}$ ,  $\dot{\theta}_{\text{eff}}$ , and  $\dot{\phi}_{\text{eff}}$  are all the corresponding velocities. Note that the  $\theta_{\text{eff}}$  and  $\phi_{\text{eff}}$  are functions dependent on Motor 1 and 2 angles (see Fig. 2 for motor number designation),  $\theta_1$  and  $\theta_2$ , as follows:

$$\phi_{\text{eff}} = \frac{\theta_1(-1)^{a+1} + \theta_{\text{eff}}}{N_\phi}, \quad \theta_{\text{eff}} = \frac{\theta_2}{N_\theta}(-1)^{b+1}, \quad (2)$$

where  $a$  is the number of gears in the worm gear assembly housed in the turret, with a gear ratio  $N_\phi$ , and  $b$  is the number

of gears in the gear train driving the turret, with a gear ratio  $N_\theta$ . The control inputs are defined as

$$\mathbf{u} = [u_1 \quad u_2]^T, \quad (3)$$

where  $u_1$  and  $u_2$  are the velocity command inputs to Motors 1 and 2, respectively.

### B. Deriving System Dynamics

Using the axes in Fig. 2, the displacement of the end of the string  $X$  assuming negligible string stretch is

$$X = r_w \phi_{\text{eff}} - \left( L_c - \sqrt{L_c^2 - \theta_{\text{eff}}^2 r_0^2} \right), \quad (4)$$

where  $L_c$  is the contracted string length,  $r_w$  is the winch radius, and  $r_0$  is the initial string radius. Equation 4 assumes there is an antagonist load that keeps the string taut. The contracted length is defined as  $L_c = L + r_w \phi_{\text{eff}}$ , with  $L$  being the uncontracted string length. Differentiating with respect to time yields

$$\dot{X} = \frac{\theta_{\text{eff}} r_0^2 \dot{\theta}_{\text{eff}} + r_w L_c \dot{\phi}_{\text{eff}}}{\sqrt{L_c^2 - \theta_{\text{eff}}^2 r_0^2}}. \quad (5)$$

### C. Control Law

This system relies on two inputs, as seen in Fig. 3. The feedback position controller (1) delivers a single control effort through a P controller and (2) distributes this control effort between twisting and winching, guided by preferences for higher force or velocity output. The tracking error is defined as  $e = X_d - \tilde{X}$ , where  $X_d$  is the desired position and  $\tilde{X}$  is the displacement measurement from the voltage of the conductive string. A conventional P-controller was used for position tracking,

$$v = K_P e, \quad (6)$$

where  $v$  is the control effort and  $K_P$  is the proportional gain. Despite the system's nonlinear characteristics, a linear controller was chosen for ease of implementation, leveraging feedback to manage nonlinearities. Furthermore, for the vast majority of operations, motion is dominated by the winch action  $r_w \theta_{\text{eff}}$ , and the system is hence mostly linear as seen in Equation 4, so a linear controller with just a proportional gain should be sufficient. Only when more twisting occurs and  $\theta_{\text{eff}}$  increases does the square root term become more influential and the system become more nonlinear, requiring a change in controller gain or other techniques such as feedback linearization. This will be discussed later in this section.

Allocating control effort between twisting and winching was done through proportional division:

$$v_{\theta s} = \beta v, \quad (7)$$

and

$$v_{\phi s} = (1 - \beta)v, \quad (8)$$

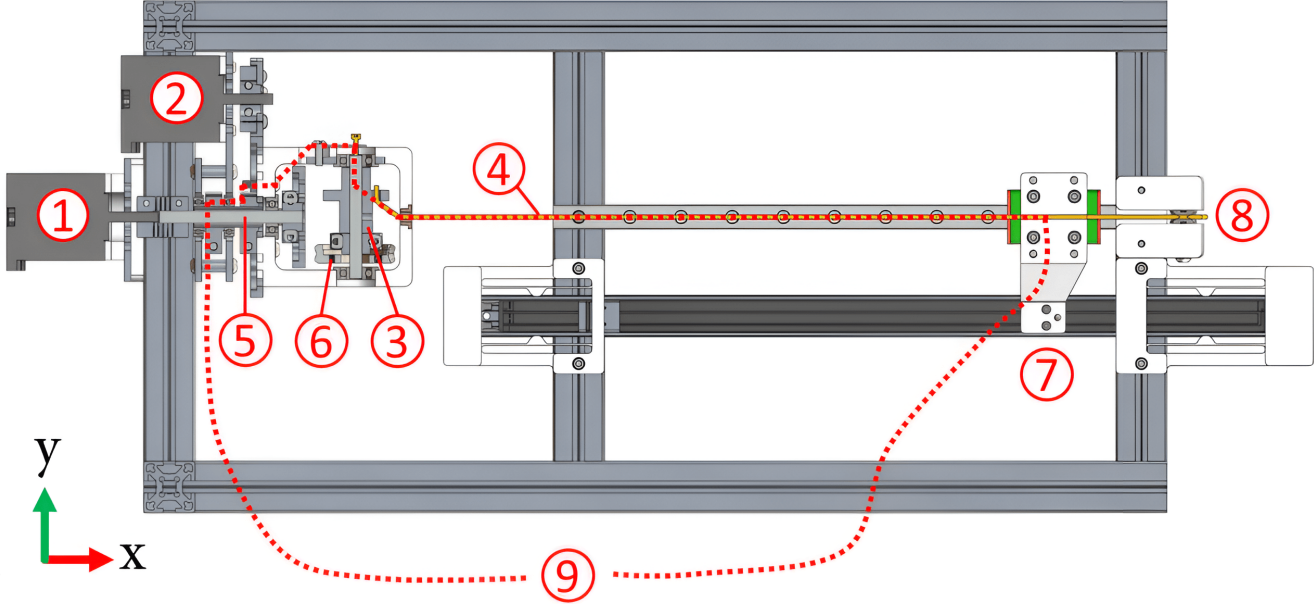


Fig. 2. Cross section of the actuator and experimental setup. Motor 2 (2) twists the string (4) by rotating the winch (3) around its radial axis. Motor 1 (1) turns a drive shaft (5) through Motor 2's gear transmission to rotate a worm gear train (6), winding up the string via the winch. The string attaches to a linear rail carriage (7) with a linear potentiometer encoder, then over the table edge (8) to a set of hanging masses. The dotted red line (9) shows the conductive path used to measure string displacement through its resistivity. The path travels through the string and the turret, and two wires are used to connect the ends to a voltage sensor mounted to the side of the setup.

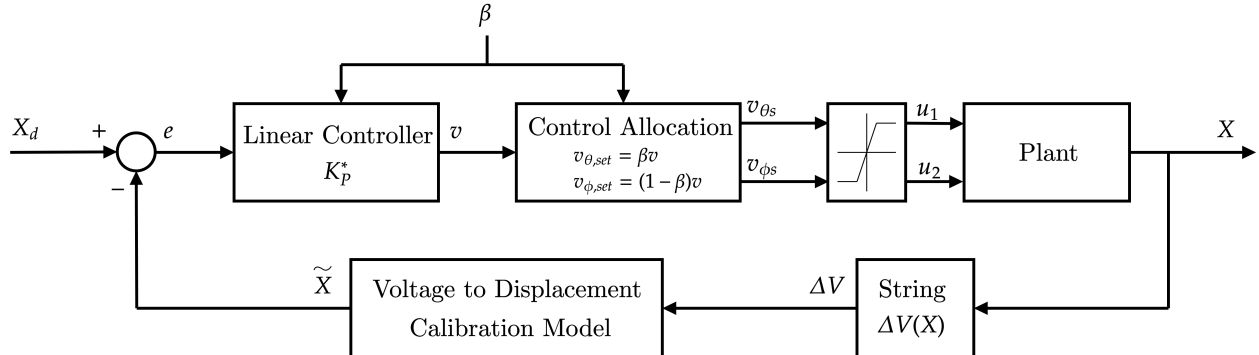


Fig. 3. Block diagram of the proposed control system. The control error  $e$  is fed to a linear controller with a gain scheduler based on the allocation factor  $\beta$ , which allocates control effort  $v$  between twisting  $v_{\theta s}$  and winching  $v_{\phi s}$ . These control efforts are hard limited and converted to motor inputs  $u_1$  and  $u_2$ . The resulting displacement  $X$  changes the voltage across the string  $\Delta V$ , which is translated into a displacement measurement  $\tilde{X}$  via a calibration model.

where  $v_{\theta s}$  and  $v_{\phi s}$  represent the control effort for twisting and winching, respectively. The factor  $\beta$  ranges from 0 to 1 and determines the balance of effort:  $\beta = 0$  allocates all control to winching, while  $\beta = 1$  directs it all to twisting. With the desired control effort allocated between twisting and winching, the motor commands can be found using Equation 2. The proposed control system can be seen in Fig. 3.

Control effort allocation is based on the fact that winching has a greater influence on velocity output, while twisting is better for maximizing force output. This is illustrated in the modified expression for the output force from [14]:

$$F_x = K \left( \sqrt{L_c^2 + \theta_{\text{eff}}^2 r_0^2} - L_c \right) \cos(\alpha) + \frac{I_\phi \ddot{\phi}}{r_w}, \quad (9)$$

where  $K$  is the string stiffness,  $I_\phi$  is the inertia of the winch about its cylindrical axis, and  $\alpha$  is the helix angle formed by the twisted string [14]. The  $I_\phi \ddot{\phi}$  term comes from the torque assuming no frictional forces. Fig. 4 compares the winch and twist contributions to velocity and force with respect to angular displacement based on Equations 5 and 9. Clearly, the winch excels at linear displacement per angle of motor rotation, while twisting has the potential to greatly

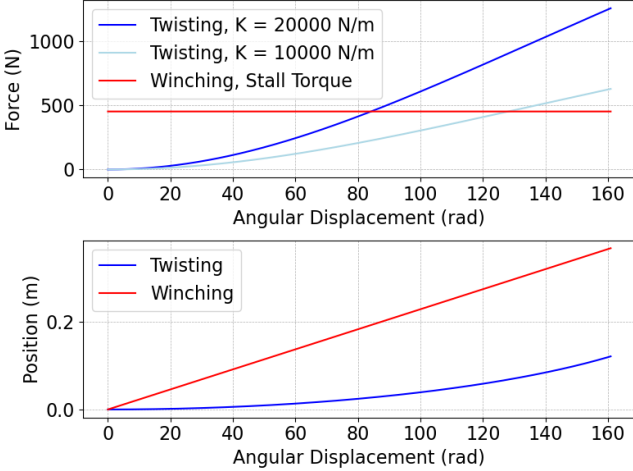


Fig. 4. Comparison of force and displacement contributions from twisting and winching. The top plot shows that twisting generates more force than winching once the twist angle  $\theta_{\text{eff}}$  exceeds a threshold, which occurs later with lower string stiffness. Winching, however, is better equipped for rapid displacement. These plots were generated using the parameters of our actuator.

exceed the limits of the stall force from winching. However, Fig. 4 also shows it is not as advantageous to use a more compliant string to generate force until a certain  $\theta_{\text{eff}}$  is reached. Nevertheless, it should be noted that the force output per unit of current drawn by the motors is most likely significantly higher for twisting, as the force from winching plotted in Fig. 4 is the force at stall.

#### D. Gain Scheduling

To achieve efficient position tracking, the controller requires different gains depending on whether it primarily uses twisting or winching. Therefore, a gain scheduling scheme was applied to the controller in Equation 6. While there are several parameters that can be used to assess performance of the gains, the scheduling schemes here were evaluated by examining the rise time in response to a step input. Rise times that are too quick typically lead to undesirable oscillations around the setpoint that reduce precision, while overly slow rise times compromise responsiveness.

For this work, an ideal rise time is on the order of seconds for setpoint tracking. The ideal rise time is shorter for trajectory tracking, where the trajectory functions for this work were discretized into smaller steps. Through simulated step responses, it was observed that as  $\beta$  shifted from 0 to 1, the gain needed for an acceptable rise time also varied. As shown in Fig. 5, using the same  $K_P$  gain through all modes  $0 \leq \beta \leq 1$  yielded step responses with rise times too fast or too slow at certain modes. Hence, the gain scheduler was made to achieve relatively similar-order rise times across all  $\beta$  for step responses and slightly faster for trajectory tracking where responsiveness to rapidly changing setpoints is more essential. The following gain scheduling scheme was devised for single step responses,

$$K_{P,\text{set}}^* = 20000\beta^2 + 100, \quad (10)$$

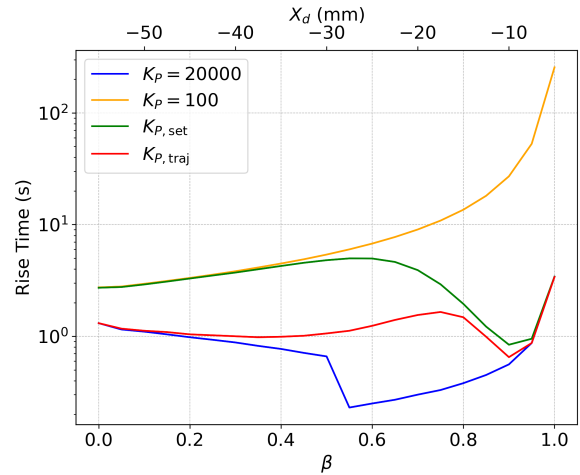


Fig. 5. Simulated relationship between  $\beta$  and rise time, where  $\beta = 0$  is pure winching and  $\beta = 1$  is pure twisting. This assumes that displacement  $|X_d|$  decreases with increasing  $\beta$ , as twisting is typically outputs more force but at lower displacements. Thus, each simulation of  $\beta$  had an assigned value of  $X_d$ , as seen in the axes above.

and for trajectory tracking,

$$K_{P,\text{traj}}^* = 100000\beta^2 + 500. \quad (11)$$

The controller in Equation 6 is thus adjusted,

$$v_{\text{set}} = K_{P,\text{set}}^* e, \quad v_{\text{traj}} = K_{P,\text{traj}}^* e. \quad (12)$$

These gain scheduling schemes were designed and evaluated numerically using simulation because it was quicker than analytically finding the step response. This would require linearizing the controller and multi-input nonlinear system defined in Equation 4 to get a transfer function. Fig. 5 shows the desired performance of the controller with the gain schedule. The system with the gain schedule of Equation 10 shows a rise times on the order of seconds, and that with the schedule of Equation 11 shows rise times slightly faster and more appropriate for trajectory tracking.

It should be noted that the desired controller gains and rise time also depend on  $X_d$ , and this gain scheduler is tailored for the expected use cases where desired displacement  $|X_d|$  decreases with rising  $\beta$ —more twist is usually done for high-force, low-displacement tasks. Nevertheless, there may be other unique cases where another controller would have to be devised.

#### E. Hard Limiter and Motor Commands

The stepper motor driver accepts step rate commands, interpreting them directly as desired velocities. Thus, the control effort outputs  $v_{\theta_s}$  and  $v_{\phi_s}$  (see Fig. 3) can be treated as velocity setpoints or scaled values thereof. To ensure twist and winch control efforts stay within motor velocity limits, the hard limiter caps the control setpoints while maintaining the proportional ratio between  $v_{\theta_s}$  and  $v_{\phi_s}$ . For instance, if  $v_{\theta_s}$  exceeds its maximum allowable velocity, then both  $v_{\theta_s}$  and  $v_{\phi_s}$  are scaled so  $v_{\theta_s}$  meets its maximum value while preserving the ratio  $\frac{v_{\phi_s}}{v_{\theta_s}}$ . Mathematically,

$$v_\phi = \begin{cases} \frac{v_{\phi_s}}{v_{\theta_s}} v_{\theta,\max} & \text{if } v_{\theta_s} > v_{\theta,\max}, v_{\phi_s} \leq v_{\phi,\max} \\ \operatorname{sgn}(v_{\phi_s}) v_{\phi,\max} & \text{if } v_{\phi_s} > v_{\phi,\max}, v_{\theta_s} \leq v_{\theta,\max} \end{cases} \quad (13)$$

$$v_\theta = \begin{cases} \operatorname{sgn}(v_{\theta_s}) v_{\theta,\max} & \text{if } v_{\theta_s} > v_{\theta,\max}, v_{\phi_s} \leq v_{\phi,\max} \\ \frac{v_{\theta_s}}{v_{\phi_s}} v_{\phi,\max} & \text{if } v_{\phi_s} > v_{\phi,\max}, v_{\theta_s} \leq v_{\theta,\max} \end{cases} \quad (14)$$

where  $v_{\theta,\max}$  and  $v_{\phi,\max}$  are the maximum twist and winch control effort velocities, governed by microstepping settings, step rate, motor resolution, and the gear ratios given in Equation 2.

If both  $v_{\theta_s}$  and  $v_{\phi_s}$  exceed their maximum values, then whichever control effort difference  $|v_{\theta_s}| - v_{\theta,\max}$  or  $|v_{\phi_s}| - v_{\phi,\max}$  is greater indicates which control effort is scaled first. For instance, if  $|v_{\theta_s}| - v_{\theta,\max}$  is greatest, then  $v_{\theta_s}$  is scaled down to maximum and  $v_{\phi_s}$  is scaled down so that  $\frac{v_{\phi_s}}{v_{\theta_s}}$  is still the same. Then, if either  $v_{\theta_s}$  and  $v_{\phi_s}$  is still above its respective maximum, the control efforts are scaled once again according to Equations 13 and 14 so the resulting  $v_\phi$  and  $v_\theta$  are at or below their maximum values. Finally, the motor commands are calculated taking the time derivative of Equation 2 to solve for  $u_1$  and  $u_2$ ,

$$u_1 = \frac{N_\phi v_\phi - v_\theta}{(-1)^{a+1}}, u_2 = \frac{N_\theta v_\theta}{(-1)^{b+1}}. \quad (15)$$

### III. SIMULATION

We simulated the system states based on controller inputs to evaluate the effect of the control allocation factor,  $\beta$ , on twist and winch velocities. Fig. 3 outlines the control strategy used, but inputs were fed into a simulated model rather than the actual plant. The constants applied in the simulation are listed in Table I.

$r_w$ [mm]	$r_0$ [mm]	$L$ [mm]	$u_{\max}$ [rad/s]
8	0.6	270	32
$N_\theta$	$N_\phi$	a	b
2	7	2	2

TABLE I  
VALUES FOR SIMULATION.

The results in Fig. 6 demonstrate that increasing  $\beta$  shifts the control effort more toward twisting, as reflected by the increased magnitude of  $v_\theta$  relative to  $v_\phi$ . The flat lines at the start indicate that the hard stops were correctly implemented. The gain scheduling scheme in Equation 10 provided reasonable rise times on the order of seconds, achieving a balance between efficiency and stability. However, the gain schedule's effectiveness depends on the target position  $X_d$ . Although Equation 10 suffices for high-twist, low-displacement and high-winch, high-displacement tasks, it may not support applications requiring both high displacement and high force.

### IV. EXPERIMENTAL SETUP AND CALIBRATION

The experimental setup (Fig. 7) consisted of two NEMA 17 motors manipulating a conductive string through twisting and winching. The string, composed of 50 strands of parallel Shieldex 117/17, was wrapped around a winch. As seen in Fig. 2, Motor 2 rotated the turret that housed the winch through a 2:1 gear reduction to twist the string. Motor 1 rotated the winch about its cylindrical axis via a through-hole drive shaft connected to a 7:1 worm gear assembly, enabling winch operation.

The string extended from the turret to a pulley that redirected the string to a hanging mass of 0.8 kg. A linear carriage clamped to the string's path was attached to a P3 America OPH Series linear potentiometer that tracked displacement. A conductive path was created by fastening a wire to the metal string clamp on the linear carriage and creating a conductive path through the turret. Wires and spring steel plates were used to maintain contact against and create a conductive path across rotating elements. The string's resistance varied from  $4.4 \Omega$  at full extension to  $1.6 \Omega$  at full contraction.

The control system used TinkerForge modules [23]. Silent Stepper bricklets drove the motors at a 1/64 microstepping resolution, powered by a 12V supply. An Analog-In bricklet measured the voltage change through the string's changing resistance and a voltage divider with a power resistor. To power the linear potentiometer, a DeWalt 20V battery was used to minimize electrical noise. All scripts were written in Python to control the system in real time, with inputs communicated directly to the TinkerForge setup.

Calibrating the string was done by first winching the string to sweep across different positions and get a model that related displacement to change in voltage. Simultaneous winching and twisting generally followed the same model as pure winching action. However, while twisting the string, the voltage-displacement model is different, most likely due to tighter string packing and better resulting conductivity.

### V. PERFORMANCE ANALYSIS

#### A. Step Response to Setpoint

Setpoint tracking and step response performance was evaluated by isolating control to either winching-only ( $\beta = 0$ ) or twisting-only ( $\beta = 1$ ) modes, comparing the actuator's response to simulated predictions (Figs. 8 and 9). This was done to test the gain scheduling scheme in Equation 10 at the extremes of  $\beta$ , where rise times would be drastically different when using a constant gain  $K_P$  but within a similar order of magnitude when using the scheduled gain  $K_{P,\text{set}}^*$ .

$\beta$	Comparison	Avg. Error [mm]	Max. Error [mm]
0	Str. vs. Sim.	-0.502	3.084
0	Str. vs. Pot.	-0.431	4.939
1	Str. vs. Sim.	0.042	0.406
1	Str. vs. Pot.	-0.056	0.481

TABLE II  
ERROR VALUES FOR SETPOINT TESTS.

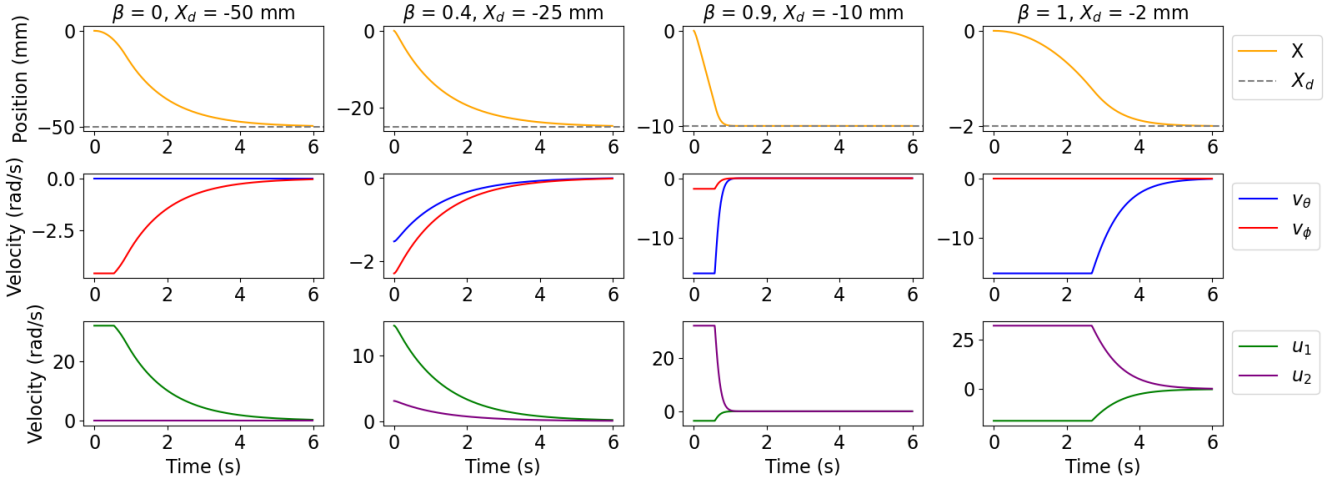


Fig. 6. Simulation results for various values of  $\beta$  and  $X_d$ . The first, second, and third rows respectively show the string displacement, twist and winch velocities, and the corresponding motor commands ( $u_1$  and  $u_2$ ).

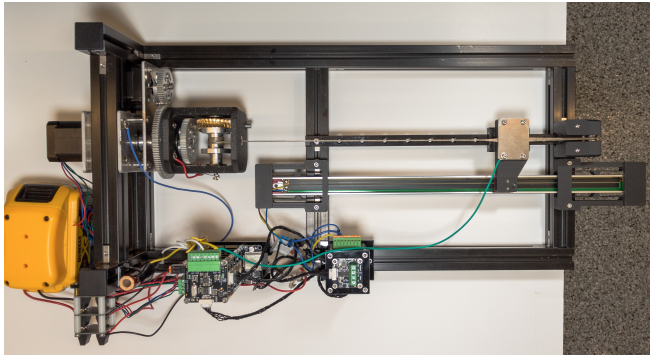


Fig. 7. Experimental setup for testing.

In winching-only mode (Fig. 8), the actuator achieved smooth and consistent tracking toward the target displacement, maintaining a close alignment between simulated and experimental results. The measured data from both the potentiometer and string sensor followed the simulation trajectory with high fidelity. The average tracking error seen in Table II of the string position relative to the simulated and actual linear potentiometer positions indicated effective control of linear motion and demonstrated the winch's capability for precise, stable displacement.

In twisting-only mode (Fig. 9), the actuator followed the setpoint with slightly greater oscillation, particularly near the endpoint. This increased variability reflected the nonlinear characteristics of twisting mechanics under load and with compliance. While the actuator converged to the target position, the average tracking error relative to the desired setpoint was slightly higher than that in winching mode, as seen in Table II. This difference highlights the additional complexity in accurately modeling twisting dynamics, particularly under conditions of high friction and stiffness. Nonetheless, the conductive string sensor provided real-time resistance feedback that effectively captured these nuances.

The results in both cases were most likely affected by the

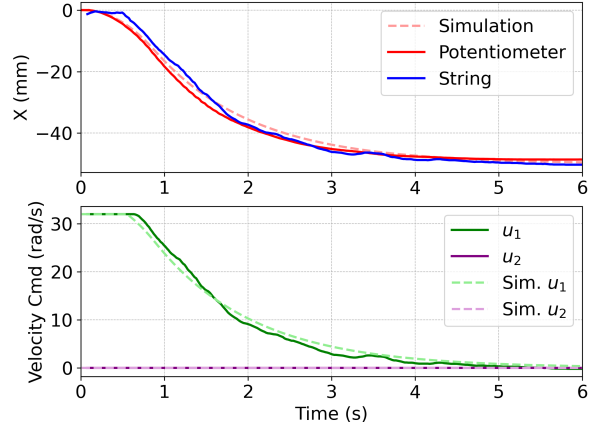


Fig. 8. Setpoint control with only winching ( $\beta = 0$ )

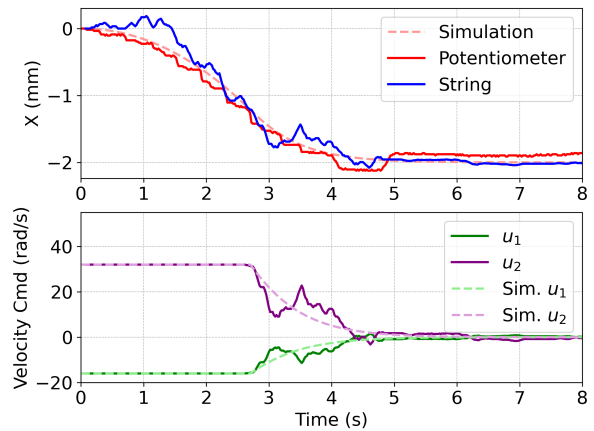


Fig. 9. Setpoint control with only twisting ( $\beta = 1$ )

$\beta$	Comparison	Avg. Error [mm]	Max. Error [mm]
0	Str. vs. Sim.	0.036	4.672
0	Str. vs. Pot.	0.576	5.086
1	Str. vs. Sim.	0.793	1.117
1	Str. vs. Pot.	1.251	1.663
0.92	Str. vs. Sim.	-3.077	4.153
0.92	Str. vs. Pot.	-1.667	4.720
Total	Str. vs. Sim.	-0.094	4.672
Total	Str. vs. Pot.	-0.096	5.086

TABLE III

ERROR VALUES FOR TRAJECTORY TESTS.

same error sources. During string manipulation, the packing of the string and failure to contain loose strands could have led to variations in voltage measurements. Additionally, the interface between rotating elements and the spring-loaded contacts might not have remained consistent throughout the tests. As the pulley winds up the string, the amount of contact between the winch surface and the string probably changed the conductive path resistance as well.

### B. Trajectory Tracking

We tested the actuator's ability to follow a trajectory typical of its intended use: first, winching for displacement ( $\beta = 0$ ); then, twisting for fine adjustment and high force output ( $\beta = 1$ ); and finally, simultaneous untwisting and unwinching ( $\beta = 0.92$ ). The piecewise trajectory function was defined as

$$X_d(t) = \begin{cases} 15\cos(t) - 4t - 15 & \text{if } t \leq 9 \\ -0.4t & \text{if } 9 < t \leq 15, \\ 7.3778t & \text{if } 15 < t \end{cases} \quad (16)$$

where  $t$  is the time in seconds, and  $X_d(t)$  is in millimeters. Between each piecewise trajectory, the current position recorded in the stepper motor driver was reset to zero.

Getting the actuator to follow the trajectory reliably and consistently proved to be challenging when using the conductive string instead of the linear potentiometer. Of the many tests, only a handful of yielded meaningful results. Most attempts were plagued by noise stemming from the same error sources in the step response tests and from the string coating wearing down over time, leading to several re-calibrations. However, the couple of successful trials demonstrated that it is possible for the hybrid actuator with a conductive string to achieve precise trajectory tracking.

Fig. 10 shows one of the better trials. In the initial winching phase, the actuator reached the target quickly, with a low average tracking error of 0.036 mm. Control was stable, with minor oscillations that dampened rapidly. Upon nearing the target, the actuator shifted to twisting, achieving finer positioning with high force motion and a tracking error of 0.793 mm. Finally, the simultaneous untwisting and unwinching tracked the desired movement with an error of -3.077 mm (Table III). Large errors with each new trajectory could be attributed to the fact that the start position of each piecewise function was not the same as simulated, but it

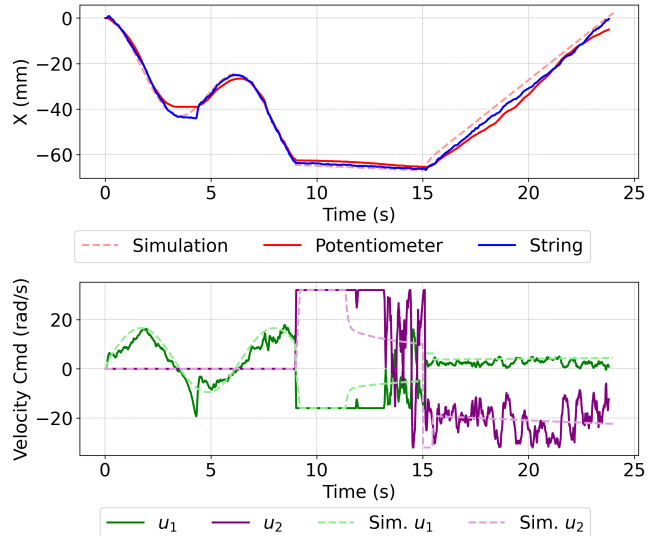


Fig. 10. One of the successful trajectory tracking tests for the expected use case: winching, twisting, then simultaneous untwisting and unwinching. It should be noted that using the conductive string for feedback during trajectory tracking was highly inconsistent due to noise.

should be pointed out that the general shape of the curves do match the desired path (Fig. 10). Furthermore, errors between the actual position recorded by the potentiometer and the string measurement seen in Table III suggests good modeling of the relationship between voltage and displacement.

## VI. CONCLUSIONS AND FUTURE WORK

We have presented a novel actuator that combines a twisted string actuator with a winch mechanism, overcoming key limitations of traditional TSAs. By integrating these two systems, we achieved greater stroke length and variable transmission ratios without risking overtorsion. Experiments validated our controller models and demonstrated the potential of using a conductive string for real-time strain measurement. This work provides users with an easily implemented method to control the actuator across different modes, delivering improved tracking performance regardless of whether a task requires high force or rapid displacement.

This hybrid actuator holds significant promise for soft robotics. Its lightweight, compact design makes it ideal for applications where adaptability and gentle interaction are crucial. For soft robotic manipulators, exoskeletons, and wearable devices, this actuator offers the ability to adjust stiffness on the fly. This flexibility allows such robots to perform complex tasks more efficiently and safely.

By combining the strengths of TSAs and winches, this versatile tool expands the capabilities of soft robotic systems. The actuator's compatibility with compliant materials and its embodied sensing align well with the core principles of soft robotics. In conclusion, our hybrid twist-winch actuator advances actuation technology and opens new avenues in soft robotics. We believe this system will contribute significantly to the development of more responsive, adaptable, and efficient robotic systems.

## A. Future Work

The TSA-winch combination offers significant advantages in stroke flexibility and force transmission, though there are several open paths for improvement. Refining the design to reduce friction and enhance efficiency could advance performance. Better modeling of the conductive string relationship between resistance and twisting angle theta would lead to better trajectory tracking across different  $\beta$  modes. Lastly, implementing adaptive control algorithms, possibly with machine learning, could enhance precision and responsiveness.

Further research will also expand on the design, address the identified limitations, and explore new applications for this innovative actuator. Exploring alternative string materials, such as those with higher conductivity or lower compliance, may offer gains in responsiveness and durability. Miniaturizing the actuator could also open new possibilities in microscale robotics or wearable devices. Investigating the scalability of the design might lead to broader adoption across different fields. Finally, integrating the actuator into practical applications—robotic grippers, exoskeletons, or soft manipulators—would test its capabilities in real-world settings. Evaluating its performance under varying loads and speeds could reveal insights into its versatility and limitations.

## REFERENCES

- [1] M. Hosseini, A. Sengül, Y. Pane, J. De Schutter, and H. Bruyninck, “Exoten-glove: A force-feedback haptic glove based on twisted string actuation system,” in *2018 27th IEEE International Symposium on Robot and Human Interactive Communication (RO-MAN)*. IEEE, 2018, pp. 320–327. [Online]. Available: <https://ieeexplore.ieee.org/abstract/document/8525637/>
- [2] S. Nedelchev, I. Gaponov, and J.-H. Ryu, “Design of robotic gripper with constant transmission ratio based on twisted string actuator: Concept and evaluation,” in *2018 IEEE/RSJ International Conference on Intelligent Robots and Systems (IROS)*. IEEE, 2018, pp. 967–972. [Online]. Available: <https://ieeexplore.ieee.org/abstract/document/8593794/>
- [3] H.-S. Seong, D.-H. Kim, I. Gaponov, and J.-H. Ryu, “Development of a twisted string actuator-based exoskeleton for hip joint assistance in lifting tasks,” in *2020 IEEE International Conference on Robotics and Automation (ICRA)*. IEEE, 2020, pp. 761–767. [Online]. Available: <https://ieeexplore.ieee.org/abstract/document/9197359/>
- [4] D. Bombara, R. Coulter, R. Konda, and J. Zhang, “A twisted string actuator-driven soft robotic manipulator,” *IFAC-PapersOnLine*, vol. 54, no. 20, pp. 141–146, 2021, publisher: Elsevier. [Online]. Available: <https://www.sciencedirect.com/science/article/pii/S2405896321022102>
- [5] J. H. Poynting, “On pressure perpendicular to the shear planes in finite pure shears, and on the lengthening of loaded wires when twisted,” *Proceedings of the Royal Society of London. Series A, Containing Papers of a Mathematical and Physical Character*, vol. 82, no. 557, pp. 546–559, Jan. 1909, publisher: Royal Society. [Online]. Available: <https://royalsocietypublishing.org/doi/10.1098/rspa.1909.0059>
- [6] ——, “The changes in length and volume of an Indian-rubber cord when twisted,” *India Rubber*, p. 6, Oct. 1906.
- [7] R. Konda and J. Zhang, “Experimental investigation of the non-smooth actuation in twisted and coiled string artificial muscles,” in *Bioinspiration, Biomimetics, and Bioreplication XIII*, vol. 12481. SPIE, Apr. 2023, pp. 43–52. [Online]. Available: <https://www.spiedigitallibrary.org/conference-proceedings-of-spie/12481/1248107/Experimental-investigation-of-the-non-smooth-actuation-in-twisted-and/10.11117/12.2657724.full>
- [8] S. H. Jeong and K.-S. Kim, “A 2-speed small transmission mechanism based on twisted string actuation and a dog clutch,” *IEEE Robotics and Automation Letters*, vol. 3, no. 3, pp. 1338–1345, 2018, publisher: IEEE. [Online]. Available: <https://ieeexplore.ieee.org/abstract/document/8253814/>
- [9] H. Singh, D. Popov, I. Gaponov, and J.-H. Ryu, “Passively adjustable gear based on twisted string actuator: Concept, model and evaluation,” in *2015 IEEE International Conference on Robotics and Automation (ICRA)*. IEEE, 2015, pp. 238–243. [Online]. Available: <https://ieeexplore.ieee.org/abstract/document/7139006/>
- [10] S. Kim, J. Sim, and J. Park, “Elastomeric continuously variable transmission combined with twisted string actuator,” *IEEE Robotics and Automation Letters*, vol. 5, no. 4, pp. 5477–5484, 2020, publisher: IEEE. [Online]. Available: <https://ieeexplore.ieee.org/abstract/document/9137664/>
- [11] J. Jang, Y.-U. Song, and J.-H. Ryu, “Active-Type Continuously Variable Transmission System Based on a Twisted String Actuator,” *IEEE Robotics and Automation Letters*, vol. 7, no. 2, pp. 2605–2612, Apr. 2022, conference Name: IEEE Robotics and Automation Letters. [Online]. Available: <https://ieeexplore.ieee.org/document/9691773/?arnumber=9691773>
- [12] S. Baek, J. Jang, and J.-H. Ryu, “Enhancing Maximum Stroke of Twisted String Actuators by Adjusting Twisting Ratio,” *IEEE Robotics and Automation Letters*, vol. 9, no. 6, pp. 5887–5894, Jun. 2024, conference Name: IEEE Robotics and Automation Letters. [Online]. Available: <https://ieeexplore.ieee.org/document/10521799/?arnumber=10521799>
- [13] T. Tsabedze, R. Konda, D. Bombara, and J. Zhang, “Model-Based Performance Analysis of Twisted String Actuators With Comparison to Spooled Motor Tendon-Driven Actuators,” *IEEE Robotics and Automation Letters*, vol. 9, no. 9, pp. 7739–7746, Sep. 2024, conference Name: IEEE Robotics and Automation Letters. [Online]. Available: <https://ieeexplore.ieee.org/document/10607867/?arnumber=10607867>
- [14] R. Poon, V. Padia, and I. W. Hunter, “A Novel Twisted-Winch String Actuator for Robotic Applications: Design and Validation,” Oct. 2024, arXiv:2410.12097. [Online]. Available: <http://arxiv.org/abs/2410.12097>
- [15] I. Gaponov, D. Popov, and J.-H. Ryu, “Twisted string actuation systems: A study of the mathematical model and a comparison of twisted strings,” *IEEE/ASME Transactions on mechatronics*, vol. 19, no. 4, pp. 1331–1342, 2013, publisher: IEEE. [Online]. Available: <https://ieeexplore.ieee.org/abstract/document/6605615/>
- [16] G. Palli, M. Hosseini, and C. Melchiorri, “Twisted string actuation with sliding surfaces,” in *2016 IEEE/RSJ International Conference on Intelligent Robots and Systems (IROS)*. IEEE, 2016, pp. 260–265. [Online]. Available: <https://ieeexplore.ieee.org/abstract/document/7759064/>
- [17] D. Bombara, R. Konda, and J. Zhang, “Experimental Characterization and Modeling of the Self-Sensing Property in Compliant Twisted String Actuators,” *IEEE Robotics and Automation Letters*, vol. 6, no. 2, pp. 974–981, Apr. 2021. [Online]. Available: <https://ieeexplore.ieee.org/document/9345383/?arnumber=9345383>
- [18] R. Konda, D. Bombara, and J. Zhang, “Overtwisting and Coiling Highly Enhance Strain Generation of Twisted String Actuators,” *Soft Robotics*, vol. 10, no. 4, pp. 760–769, Aug. 2023. [Online]. Available: <https://www.liebertpub.com/doi/10.1089/soro.2021.0079>
- [19] T. Helps, M. Taghavi, S. Wang, and J. Rossiter, “Twisted Rubber Variable-Stiffness Artificial Muscles,” *Soft Robotics*, vol. 7, no. 3, pp. 386–395, Jun. 2020. [Online]. Available: <https://www.liebertpub.com/doi/10.1089/soro.2018.0129>
- [20] D. Bombara, S. Fowzer, and J. Zhang, “Compliant, Large-Strain, and Self-Sensing Twisted String Actuators,” *Soft Robotics*, vol. 9, no. 1, pp. 72–88, Feb. 2022. [Online]. Available: <https://www.liebertpub.com/doi/10.1089/soro.2020.0086>
- [21] G. Palli, C. Natale, C. May, C. Melchiorri, and T. Wurtz, “Modeling and control of the twisted string actuation system,” *IEEE/ASME Transactions on Mechatronics*, vol. 18, no. 2, pp. 664–673, 2012, publisher: IEEE. [Online]. Available: <https://ieeexplore.ieee.org/abstract/document/6140578/>
- [22] S. Nedelchev, I. Gaponov, and J.-H. Ryu, “Accurate Dynamic Modeling of Twisted String Actuators Accounting for String Compliance and Friction,” *IEEE Robotics and Automation Letters*, vol. 5, no. 2, pp. 3438–3443, Apr. 2020, conference Name: IEEE Robotics and Automation Letters. [Online]. Available: <https://ieeexplore.ieee.org/abstract/document/8976141>
- [23] “Home | Tinkerforge.” [Online]. Available: <https://www.tinkerforge.com/en/>